

# Deep Image Clustering with Tensor Kernels and Unsupervised Companion Objectives

Daniel J. Trosten<sup>1</sup>, Michael C. Kampffmeyer<sup>2</sup>, Robert Jenssen<sup>2</sup>

**Abstract**—In this paper we develop a new model for deep image clustering, using convolutional neural networks and tensor kernels. The proposed Deep Tensor Kernel Clustering (DTKC) consists of a convolutional neural network (CNN), which is trained to reflect a common cluster structure at the output of its intermediate layers. Encouraging a consistent cluster structure throughout the network has the potential to guide it towards meaningful clusters, even though these clusters might appear to be nonlinear in the input space. The cluster structure is enforced through the idea of unsupervised companion objectives, where separate loss functions are attached to layers in the network. These unsupervised companion objectives are constructed based on a proposed generalization of the Cauchy-Schwarz (CS) divergence, from vectors to tensors of arbitrary rank. Generalizing the CS divergence to tensor-valued data is a crucial step, due to the tensorial nature of the intermediate representations in the CNN.

Several experiments are conducted to thoroughly assess the performance of the proposed DTKC model. The results indicate that the model outperforms, or performs comparable to, a wide range of baseline algorithms. We also empirically demonstrate that our model does not suffer from objective function mismatch, which can be a problematic artifact in autoencoder-based clustering models.

**Index Terms**—Deep clustering, image clustering, tensor kernels, Cauchy-Schwarz divergence, information theoretic learning, unsupervised companion objectives

## I. INTRODUCTION

Deep clustering is a subfield of deep learning [1] which considers the design of unsupervised loss functions, in order to train deep learning models for clustering. The loss functions developed in this field have made it possible to train deep architectures to discover underlying group structure in large datasets, containing data types with complex geometrical structure, such as images [2, 3, 4] and time series [5]. The ever growing amount of unlabeled data has caused unsupervised learning to be identified as a main next goal in machine learning research [1].

Many of the recent deep clustering models include deep neural networks that have been pre-trained as autoencoders [6, 7, 8, 9].

<sup>1</sup>Norconsult Informasjonssystemer AS.

<sup>2</sup>Department of Physics and Technology, UiT The Arctic University of Norway.

All authors are affiliated with the UiT Machine Learning Group: <https://machine-learning.uit.no>.

This work was partially funded by the Research Council of Norway grant no. 303514.

Our DTKC implementation is available at <https://github.com/DanielTrosten/DTKC>.

In these models, the unsupervised clustering loss is attached to the code space of the autoencoder, and the model is fine tuned using either the clustering loss alone, or both the clustering loss, and the reconstruction loss from the autoencoder.

Despite the popularity of the autoencoder approach, we hypothesize that the representation produced by the autoencoder does not necessarily emphasize properties which are desirable for clustering. These models can therefore suffer from *objective function mismatch* [10]. An example of this was shown in [10], where the classification performance of features produced by a variational autoencoder (VAE) sharply decreased in later stages of training, even though the loss of the VAE continued to decrease.

The use of autoencoders in deep clustering algorithms is mainly rooted in the fact that some loss functions are incapable of retaining input similarities during training [7]. Thus, training deep models with these loss functions, without the accompanied autoencoder, could result in clusters which do not reflect the similarity structure of the input space. The autoencoder can therefore be regarded as a form of regularization technique, included to preserve the input data similarities throughout the network.

In this work we develop an alternate approach to preservation of similarity structure in deep clustering. We combine our approach with a convolutional neural network (CNN) [11], to construct a model for image clustering, which we name Deep Tensor Kernel Clustering (DTKC). Our approach to similarity preservation is based on *tensor kernels* [12], as a natural consequence of the tensorial nature of the CNN’s intermediate representations. Our key contributions are summarized as follows:

- We propose the *unsupervised companion objectives*, which are objective (loss) functions attached to the output of intermediate layers in the neural network of a deep clustering model – similarly to the supervised companion objectives introduced in [13]. The unsupervised companion objectives are designed to encourage a persistent clustering structure throughout the network, potentially allowing for better preservation of input similarities and improved clustering performance.

In order to make the unsupervised companion objectives compatible with the intermediate outputs of a CNN, we leverage a connection between tensor theory and CNNs. This allows us to use tensor kernels [12] to describe the similarities between feature maps in the intermediate representations in a CNN.

- We use the unsupervised companion objectives to construct a new model for deep image clustering. The proposed DTKC consists of a CNN with the unsupervised companion objectives attached to its intermediate outputs, coupled with the clustering loss function from Deep Divergence-based Clustering (DDC) [4]. Our experiments show that DTKC outperforms DDC on almost all benchmark datasets.

The rest of the paper is structured as follows: Section II describes some of the recent advances in the field of deep clustering, followed by an overview of the relevant parts of DDC in Section III. Section IV introduces our contributions and the relevant background material. The experiments are described in Section V, followed by a hyperparameter analysis in Section VI, and a qualitative analysis of feature importance in Section VII. In Section VIII we validate our hypothesis of objective function mismatch in a convolutional autoencoder. Finally, some concluding remarks are provided in Section IX. We also include some results with recurrent neural networks and sequential data in Appendix A, to emphasize the generalizability of the unsupervised companion objectives.

## II. RELATED WORK

Deep clustering models generally adhere to the following design pattern: Take a deep neural network, and combine it with a *clustering module*, which computes the cluster membership vectors based on the representation provided by the neural network. The network and the clustering module are then trained simultaneously by minimizing an unsupervised loss function, to determine their respective parameters. The joint optimization causes the network to learn features that are well suited for the clustering module, while the clustering module learns to cluster these features in an optimal way. Most models described in the following are instances of this general framework. Since DTKC also follows this design strategy, these are the most relevant models for comparison with DTKC.

*Deep Embedded Clustering (DEC) [6]:* DEC uses a multilayer perceptron (MLP) with a clustering module based on soft-assignments to a set of centroids. The soft assignments of embedded observations are computed using a  $t$ -distribution with 1 degree of freedom. DEC’s loss function is constructed to force the distribution of soft cluster assignments closer to a target distribution, by means of the Kullback-Leibler (KL) divergence. The target distribution is constructed from the soft assignments, and is designed to strengthen predictions, put more emphasis on high-confidence assignments, and normalize the contribution of each centroid to the loss function. DEC is trained by first initializing the MLP as a stacked autoencoder, and then fine tuned using the clustering loss.

*Improved Deep Embedded Clustering (IDEC) [7]:* As the name implies, IDEC is closely related to the previously described DEC algorithm. However, the authors of IDEC argue that the fine-tuning stage of DEC results in non-representative features and thereby worse clustering performance [7]. To alleviate this IDEC keeps the decoder-part of the autoencoder during

fine-tuning, in contrast to DEC, where it is discarded. The other parts of the IDEC model are shared with DEC.

*Deep Clustering Network (DCN) [8]:* This method is also similar to IDEC, since it uses an autoencoder with a clustering module attached to the code-space. However, instead of the soft clustering module used by IDEC, DCN uses a hard  $k$ -means clustering module to produce the cluster assignments. Due to the non-differentiability of the hard cluster assignments, a three-stage optimization procedure is used to train DCN.

*SpectralNet [14]:* SpectralNet offers a deep learning based approach to the well known Spectral Clustering algorithm [15]. The model consists of a deep neural network trained to minimize the Spectral Clustering loss function, resulting in an approximation to the eigenspace mapping obtained in ordinary Spectral Clustering.

*Discriminatively Boosted image Clustering (DBC) [9]:* DBC is another autoencoder-based algorithm which is designed specifically for image clustering. It uses a fully-convolutional autoencoder, which is an autoencoder consisting of only convolutional layers [16, 17]. DBC’s training procedure starts with pre-training the autoencoder, and when the pre-training finishes, the decoder is discarded, and the encoder is fine-tuned using the clustering loss from DEC.

*Other methods:* Lastly, the deep clustering literature also contains a few algorithms that do not directly adhere to the “DNN + clustering module” framework. These algorithms include: (i) Joint Unsupervised Learning (JULE) [2], which uses a CNN for hierarchical clustering; (ii) Information Maximizing Self-Augmented Training (IMSAT) [3], which depends heavily on data augmentation; (iii) Variational Deep Embedding (VaDE) [18], which is a generative model based on variational autoencoders [19]; (iv) Categorical Generative Adversarial Network (CatGAN) [20], which is another generative model based on generative adversarial networks [21]; and (v) ClusterGAN [22], which too is based on generative adversarial networks. However, the consideration of these methods falls outside the scope of this paper, as our focus is on algorithms consisting of a DNN coupled with a clustering module.

## III. DEEP DIVERGENCE-BASED CLUSTERING

This section will give a brief description of Deep Divergence-based Clustering (DDC) [4], as we have chosen to build our proposed DTKC with components from the DDC framework. DDC was chosen primarily due to its image clustering performance, and end-to-end trainability.

The DDC model can be summarized as follows: Suppose we have a set of images  $\mathbf{X}_1, \dots, \mathbf{X}_n$ , and pass these through a CNN, followed by a vectorization step, and a fully-connected layer, resulting in the vectorial representations  $z_1, \dots, z_n$ . These representations are then processed by a final fully-connected layer with a softmax activation function, producing the predicted cluster membership vectors  $u_1, \dots, u_n$ .

DDC’s loss function is constructed based on both the representations  $z$ , and the cluster membership vectors  $u$ . It is designed to enforce the following requirements:

- (i) *Cluster compactness and separability*: In the representation space, individual clusters should be compact, while different clusters should be well separated.
- (ii) *Orthogonal cluster membership vectors*: Cluster membership vectors pointing to different clusters should be orthogonal in  $\mathbb{R}^k$ .
- (iii) *Closeness to simplex corner*: Each cluster membership vector should be close to a corner of the standard simplex in  $\mathbb{R}^k$  (defined as:  $\{(a_1, \dots, a_k) \in \mathbb{R}_{\geq 0}^k : \sum_{i=1}^k a_i = 1\}$ ).

The loss function is the sum of three terms, each of which tackles one of the properties outlined above:

$$\mathcal{L}_{\text{DDC}} = \mathcal{L}_1 + \mathcal{L}_2 + \mathcal{L}_3.$$

The first loss term enforces the separability and compactness condition through the Cauchy-Schwarz (CS) divergence between  $k$  probability density functions  $p_1, \dots, p_k$  [23]<sup>1</sup>:

$$D_{cs}(p_1, \dots, p_k) = -\ln \left( \frac{1}{k} \sum_{i=1}^{k-1} \sum_{j=i+1}^k \frac{\int p_i(z)p_j(z)dz}{\sqrt{\int p_i^2(z)dz \int p_j^2(z)dz}} \right).$$

Maximizing  $D_{cs}$  corresponds to minimizing the argument of the logarithm, resulting in:

$$\mathcal{L}_1 = \frac{1}{k} \sum_{i=1}^{k-1} \sum_{j=i+1}^k \frac{\int p_i(z)p_j(z)dz}{\sqrt{\int p_i^2(z)dz \int p_j^2(z)dz}}.$$

Suppose that each of the probability density functions represent their own cluster. The numerator of term  $(i, j)$  in  $\mathcal{L}_1$  is the integrated overlap between clusters  $i$  and  $j$ . A small value of the integrated overlap leads to clusters that are well separated. The denominator is the product of integrated self-overlap for clusters  $i$  and  $j$ . These quantities will be large if both clusters are compact. Hence, a combination of compact and well-separated clusters will result in  $\mathcal{L}_1$  taking a small value.

In general, we do not know the probability density functions  $p_1, \dots, p_k$ , and thus, they have to be estimated from data. Using the kernel density estimator [24] we get<sup>2</sup>:

$$p_j(z) = \frac{1}{|\mathcal{C}_j| \sigma^{\dim Z}} \sum_{z_j \in \mathcal{C}_j} K \left( \frac{\|z - z_j\|}{\sigma} \right)$$

where  $K$  is chosen to be a Gaussian

$$K(x) = \frac{1}{\sqrt{2\pi}} \exp \left( -\frac{x^2}{2} \right)$$

and  $\sigma$  is a bandwidth parameter. If we assume for now, that the cluster membership functions produce hard assignments, we can rewrite  $\mathcal{L}_1$  as:

$$\mathcal{L}_1 = \frac{1}{k} \sum_{i=1}^{k-1} \sum_{j=i+1}^k \frac{\mathbf{v}_i^T \mathbf{K} \mathbf{v}_j}{\sqrt{\mathbf{v}_i^T \mathbf{K} \mathbf{v}_i \mathbf{v}_j^T \mathbf{K} \mathbf{v}_j}}$$

<sup>1</sup>Note that  $\frac{1}{k}$  is used as a normalization constant, instead of  $\binom{k}{2}^{-1}$ , which was used in [23]. In order to describe DDC in its original form, we will stick to  $\frac{1}{k}$  in this section.

<sup>2</sup>Note the small abuse of notation where  $p_j$  denotes both the true pdf and the kernel density estimate.

where  $\mathbf{K} = [\kappa_{ij}]$  is the kernel matrix whose elements are the pairwise similarities between the outputs of the first fully-connected layer:  $\kappa_{ij} = K \left( \frac{\|z_i - z_j\|}{\sigma} \right)$ .  $\mathbf{v}_j$  denotes the  $j$ -th column of the  $n \times k$  cluster assignment matrix  $\mathbf{U}$ , which can be formed row-wise from the cluster assignment vectors  $\mathbf{u}_1, \dots, \mathbf{u}_n$ . To make the loss function differentiable, we can now relax the hard membership constraint, and allow for soft assignments instead.

The second loss term enforces the orthogonality between the cluster assignments vectors  $\mathbf{u}_1, \dots, \mathbf{u}_n$ . The matrix  $\mathbf{U}\mathbf{U}^T$  consist of pairwise inner products between cluster assignment vectors, and thus, small elements in the upper (or lower) triangular part of this matrix would correspond to orthogonal cluster assignment vectors. This gives the loss term

$$\mathcal{L}_2 = \text{triu}(\mathbf{U}\mathbf{U}^T) = \sum_{i=1}^{n-1} \sum_{j=i+1}^n \mathbf{u}_i^T \mathbf{u}_j$$

which is the sum of the strictly upper triangular part of  $\mathbf{U}\mathbf{U}^T$ . However, this sum also enforces orthogonality between vectors pointing to the same cluster, and thus introduces a regularizing effect to the optimization by repelling the cluster assignment vectors away from each other.

The last loss term ensures that the cluster assignment vectors lie close to a corner of the simplex containing the assignments  $\mathbf{u}_1, \dots, \mathbf{u}_n$ . Let  $\mathbf{M}$  be the matrix whose elements are:

$$m_{ij} = \exp(-\|\mathbf{u}_i - \mathbf{e}_j\|^2)$$

where  $\mathbf{e}_j$  denotes the  $j$ -th corner of the simplex ( $j$ -th cartesian basis vector). Then we have the loss term:

$$\mathcal{L}_3 = \frac{1}{k} \sum_{i=1}^{k-1} \sum_{j=i+1}^k \frac{\mathbf{m}_i^T \mathbf{K} \mathbf{m}_j}{\sqrt{\mathbf{m}_i^T \mathbf{K} \mathbf{m}_i \mathbf{m}_j^T \mathbf{K} \mathbf{m}_j}}$$

where  $\mathbf{m}_j$  denotes the  $j$ -th column of  $\mathbf{M}$ . Due to its resemblance to  $\mathcal{L}_1$ ,  $\mathcal{L}_3$  can be interpreted analogously: The distribution of cluster assignment vectors should be compactly centered around separate simplex corners.

The DDC architecture is then trained to minimize  $\mathcal{L}_{\text{DDC}}$  using stochastic mini-batch gradient descent.

#### IV. DEEP TENSOR KERNEL CLUSTERING

This section provides the details on the proposed unsupervised companion objectives and the DTKC model. It starts with a review of the relevant background material on tensors and tensor kernels, followed by the derivation of the unsupervised companion objectives for tensors of arbitrary rank, and an overview of DTKC.

##### A. Tensors and tensor kernels

In order to develop the proposed unsupervised companion objectives, the notions of cluster compactness and separability discussed in the preceding section have to be generalized such that they can be applied to the intermediate representations

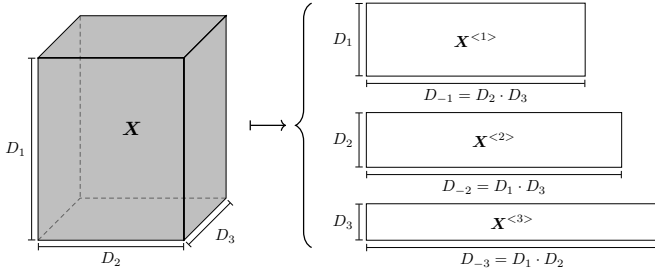


Figure 1: Matricization of a rank-3 tensor  $\mathbf{X}$ .

of a CNN. We do this through a natural connection between CNNs and tensor theory, where the feature maps produced by a convolutional layer for a single image is regarded as a rank-3 tensor in a given basis. In the following, we will use this idea together with *tensor kernels* [12] to incorporate cluster compactness and separability into our unsupervised companion objectives.

1) *The naïve kernel*: Recall that for rank-1 tensors (vectors) we have the Gaussian kernel:

$$k_\sigma(\mathbf{x}, \mathbf{y}) = \exp\left(-\frac{\|\mathbf{x} - \mathbf{y}\|^2}{2\sigma^2}\right) = \prod_{i=1}^{D_1} \exp\left(-\frac{(x_i - y_i)^2}{2\sigma^2}\right)$$

where  $x_i$  ( $y_i$ ) refers to element  $i$  in the vector  $\mathbf{x}$  ( $\mathbf{y}$ ). The latter equality shows that this kernel belongs to a particular class of kernels, namely *product kernels*. Generalizing this kernel to tensors  $\mathbf{X}$  and  $\mathbf{Y}$  of rank  $r$  gives the naïve kernel [12]:

$$k_\sigma^{\text{naïve}}(\mathbf{X}, \mathbf{Y}) = \prod_{i_1=1}^{D_1} \cdots \prod_{i_r=1}^{D_r} \exp\left(-\frac{(X_{i_1 \dots i_r} - Y_{i_1 \dots i_r})^2}{2\sigma^2}\right)$$

where  $X_{i_1 \dots i_r}$  ( $Y_{i_1 \dots i_r}$ ) denotes the element of  $\mathbf{X}$  ( $\mathbf{Y}$ ) with indices  $i_1, \dots, i_r$ , and  $D_1, \dots, D_r$  denote the number of elements along each dimension. This kernel has *kernel components* for all elements in the product, which are used to form the product kernel. However, as is also pointed out in [12], this causes the kernel function to ignore the local structure within and between the respective tensors, due to the commutativity of multiplication. Mathematically, this means that the kernel is invariant to a fixed permutation rule  $P$ :

$$k_\sigma^{\text{naïve}}(\mathbf{X}, \mathbf{Y}) = k_\sigma^{\text{naïve}}(P(\mathbf{X}), P(\mathbf{Y})).$$

This effect can be especially destructive for images, for instance, since images can be transformed beyond recognition by permuting the spatial indices.

2) *Matricization-based tensor kernels*: The problem outlined above calls for a more robust kernel which takes local structure into account. To this end, it was suggested in [12] to define a product kernel over the *matricizations* of the input tensors:

$$k_\sigma^{\text{tensor}}(\mathbf{X}, \mathbf{Y}) = \prod_{m=1}^r k_\sigma^m(\mathbf{X}^{<m>}, \mathbf{Y}^{<m>})$$

where  $\mathbf{X}^{<m>}$  is the matricization of  $\mathbf{X}$  along dimension  $m$  (and similarly for  $\mathbf{Y}$ ).

Figure 1 shows an example of the matricization process where the rank-3 tensor  $\mathbf{X}$  is transformed to the matrices

$\mathbf{X}^{<1>}$ ,  $\mathbf{X}^{<2>}$  and  $\mathbf{X}^{<3>}$ . In this case the tensor  $\mathbf{X}$  could be an image, or the output of a convolutional layer in a CNN – the latter being the connection between tensors and CNNs mentioned earlier.

Thus, it remains to specify the form of the components  $k_\sigma^m(\cdot, \cdot)$ , in the product kernel. We will stick to the Gaussian kernel, but use a distance function on the *Grassmann manifold* spanned by the respective matricizations (see Figure 2). Considering data matrices as points on the Grassmann manifold is the key concept in *Grassmannian learning* [25, 26, 27]. Results from this field indicate that using a distance function on the Grassmann manifold tends to improve performance of distance-based machine learning systems for tensor data [26, 27].

If we couple the Gaussian kernel with a generic distance function  $d_{\mathcal{G}(D_m, D_{-m})}$  on the Grassmann manifold, we get the kernel component:

$$k_\sigma^m(\mathbf{X}^{<m>}, \mathbf{Y}^{<m>}) = \exp\left(-\frac{d_{\mathcal{G}(D_m, D_{-m})}(\mathbf{X}^{<m>}, \mathbf{Y}^{<m>})^2}{2\sigma^2}\right).$$

Here  $\mathcal{G}(D_m, D_{-m})$  denotes the Grassmann manifold, which consists of all  $D_m$ -dimensional linear subspaces of  $\mathbb{R}^{D_{-m}}$ , where  $D_{-m} = D_1 \cdots D_{m-1} \cdot D_{m+1} \cdots D_r$ . This interpretation of the matricizations assumes that we have  $D_m \leq D_{-m}$ , as the dimensionality of the subspace has to be less than or equal to the dimensionality of the parent-space. This assumption does not necessarily hold for general tensors, which means that the computations have to take this into account to ensure the correctness of the approach. Matricizations for which  $D_m > D_{-m}$  are therefore transposed prior to the distance computation, following [12], meaning that we essentially consider distances on  $\mathcal{G}(D_{-m}, D_m)$  instead. Throughout the rest of this paper we will assume that  $D_m < D_{-m}$ , and that the transposition has been made whenever this does not hold.

Note that it is not the matrix  $\mathbf{X}^{<m>}$  itself that lies on the Grassmann manifold, but rather the span of its rows. Therefore, it is useful to represent points on the manifold as  $D_m \times D_{-m}$  orthonormal matrices, whose rows are orthogonal unit-length vectors which together form an orthogonal basis for the linear subspace. These orthonormal representations can be obtained through the compact singular value decomposition (SVD) of the original input matrices. For a real matricization  $\mathbf{X}^{<m>}$  with shape  $(D_m, D_{-m})$  satisfying  $D_m < D_{-m}$ , we have

$$\mathbf{X}^{<m>} = \mathbf{U}_X^{<m>} \boldsymbol{\Sigma}_X^{<m>} (\mathbf{V}_X^{<m>})^T \quad (1)$$

where  $\boldsymbol{\Sigma}_X^{<m>}$  is a diagonal matrix with shape  $(D_m, D_m)$  and nonnegative real numbers on the diagonal.  $\mathbf{U}_X^{<m>}$  and  $\mathbf{V}_X^{<m>}$  are orthonormal matrices with shapes  $(D_m, D_m)$  and  $(D_{-m}, D_m)$  respectively. Moreover, it can be shown that the row span of  $(\mathbf{V}_X^{<m>})^T$  is equal to the row span of  $\mathbf{X}^{<m>}$  [28]. Thus one can take  $(\mathbf{V}_X^{<m>})^T$  to be the orthonormal representation of  $\mathbf{X}^{<m>}$ .

In the following, we will use these orthonormal representations to compute distances on the Grassmann manifold. The distance computation is illustrated in Figure 2.

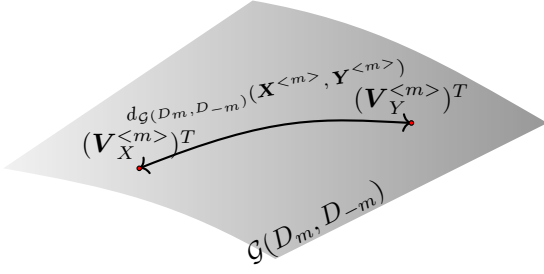


Figure 2: The distance  $d_{\mathcal{G}(D_m, D-m)}(\mathbf{X}^{<m>}, \mathbf{Y}^{<m>})$  between two matricizations  $\mathbf{X}^{<m>}$  and  $\mathbf{Y}^{<m>}$  on the Grassmann manifold  $\mathcal{G}(D_m, D-m)$ . Since the Grassmann manifold consists of linear subspaces, the matricizations are represented by the respective orthonormal representations  $(\mathbf{V}_X^{<m>})^T$  and  $(\mathbf{V}_Y^{<m>})^T$ .

3) *Distance functions on Grassmann manifolds:* There exists a variety of different distance functions on Grassmann manifolds in the literature [25, 27]. Among the most commonly used distances, we find the geodesic (arc length) distance, and the projection distance. However, the former is computed using the principal angles between the respective subspaces [25]. The computation of these angles requires another SVD, which substantially increases the computational cost of the distance computations. Moreover, it can be shown that a Gaussian kernel using the geodesic distance is not positive semidefinite [26]. Conversely, the projection distance does not require another SVD to be computed, and when coupled with a Gaussian, it results in a positive semidefinite kernel [26]. The projection distance function is based on the *orthogonal projection operator* which takes an arbitrary element of  $\mathbb{R}^{D-m}$  and projects it orthogonally to the subspace spanned by the matricization. For a matricization  $\mathbf{X}^{<m>}$ , the projection operator is given by the product  $\mathbf{V}_X^{<m>}(\mathbf{V}_X^{<m>})^T$  [12]. Considering the Frobenius norm between projection operators gives the distance function:

$$d_{\mathcal{G}(D_m, D-m)}^{\text{proj}}(\mathbf{X}^{<m>}, \mathbf{Y}^{<m>}) = \|\mathbf{V}_X^{<m>}(\mathbf{V}_X^{<m>})^T - \mathbf{V}_Y^{<m>}(\mathbf{V}_Y^{<m>})^T\|_F$$

where  $\|\cdot\|_F$  denotes the Frobenius norm. Moreover, it can be shown that:

$$d_{\mathcal{G}(D_m, D-m)}^{\text{proj}}(\mathbf{X}^{<m>}, \mathbf{Y}^{<m>}) = \sqrt{2(D_m - \text{tr}((\mathbf{V}_Y^{<m>})^T \mathbf{V}_X^{<m>} (\mathbf{V}_X^{<m>})^T \mathbf{V}_Y^{<m>}))}$$

which is more efficient to compute compared to the previous expression [12].

Using the projection distance, we obtain the tensor kernel:

$$k_{\sigma}^{\text{tensor}}(\mathbf{X}, \mathbf{Y}) = \prod_{m=1}^r \exp\left(-\frac{d_{\mathcal{G}(D_m, D-m)}^{\text{proj}}(\mathbf{X}^{<m>}, \mathbf{Y}^{<m>})^2}{2\sigma^2}\right).$$

Due to the positive semidefiniteness of the product kernels, this kernel is also positive semidefinite [26].

## B. Unsupervised companion objectives

In this subsection we describe the proposed unsupervised companion objectives, which offer a new approach to the design of unsupervised loss functions. The method is similar in spirit to the supervised companion objectives introduced in [13], where a classifier was attached to each layer of the network, in order to increase the overall classification performance of the model.

Suppose we have the following deep clustering setup:

$$\mathbf{z} = f_{\theta}(\mathbf{X}), \quad \mathbf{u} = g_{\phi}(\mathbf{z})$$

where  $f_{\theta}$  denotes the neural network producing the learned representation  $\mathbf{z}$ , from the input  $\mathbf{X}$ , and  $g_{\phi}$  denotes the clustering module producing the cluster membership vector  $\mathbf{u}$ .  $\theta$  and  $\phi$  denote the parameters of the neural network, and the parameters of the clustering module, respectively. Since  $f_{\theta}$  represents a neural network, it can be decomposed *block-wise* as:

$$f_{\theta} = f_{\theta_L}^L \circ f_{\theta_{L-1}}^{L-1} \circ \dots \circ f_{\theta_1}^1$$

where  $f_{\theta_l}^l$  is the mapping performed by block  $l$ , and  $L$  is the number of blocks. We will throughout this paper refer to blocks as generic computational units in a deep neural network. Layers are the most familiar examples of blocks, but a block can also represent, for instance, a collection of adjacent layers, or individual components within a specific layer.

If we let  $\mathbf{Y}^l$  be the output of block  $l$ , we have:

$$\mathbf{Y}^l = f_{\theta_l}^l(\mathbf{Y}^{l-1})$$

with  $\mathbf{Y}^0 = \mathbf{X}$  and  $\mathbf{Y}^L = \mathbf{z}$ . Note that we assume  $\mathbf{X}$  and  $\mathbf{Y}^1, \dots, \mathbf{Y}^{L-1}$  to be tensors of arbitrary rank, whereas  $\mathbf{z}$  and  $\mathbf{u}$  are assumed to be vectors (rank-1 tensors).

For a tensor-valued dataset  $\mathcal{X} = \{\mathbf{X}_1, \dots, \mathbf{X}_n\}$ , our proposed loss function then reads:

$$\mathcal{L} = \mathcal{L}_{\text{DDC}}(\mathcal{X}, \theta, \phi) + \lambda \sum_{l=1}^{L-1} \mathcal{L}_{\text{co}}^l(\mathbf{Y}_1^l, \dots, \mathbf{Y}_n^l, \mathbf{U}) \quad (2)$$

where  $\mathcal{L}_{\text{DDC}}$  is the clustering loss function from DDC, and  $\mathcal{L}_{\text{co}}^l(\mathbf{Y}_1^l, \dots, \mathbf{Y}_n^l, \mathbf{U})$  is the unsupervised companion objective for the  $l$ -th block. The companion objective for a specific block depends on both the outputs of that block ( $\mathbf{Y}_1^l, \dots, \mathbf{Y}_n^l$ ) and the cluster membership matrix produced by the clustering module.  $\lambda$  is a hyperparameter which determines the strength of the companion objectives.

$\mathcal{L}_{\text{co}}^l$  should be designed to enforce a discriminative cluster structure at block  $l$  in the network. Using the CS divergence, we get the companion objective:

$$\mathcal{L}_{\text{co}}^l(\mathbf{Y}_1^l, \dots, \mathbf{Y}_n^l, \mathbf{U}) = \frac{1}{\binom{k}{2}} \sum_{i=1}^{k-1} \sum_{j=i+1}^k \frac{\mathbf{v}_i^T \mathbf{K}^l \mathbf{v}_j}{\sqrt{\mathbf{v}_i^T \mathbf{K}^l \mathbf{v}_i \mathbf{v}_j^T \mathbf{K}^l \mathbf{v}_j}} \quad (3)$$

where  $k$  is the number of clusters,  $\mathbf{v}_i$  denotes the  $i$ -th *column* of the cluster membership matrix  $\mathbf{U}$ , and  $\mathbf{K}^l = [\kappa_{ij}^l]$  is a kernel matrix whose elements are:

$$\kappa_{ij}^l = k_{\sigma}^{\text{tensor}}(\mathbf{Y}_i^l, \mathbf{Y}_j^l)$$

where  $k_\sigma^{\text{tensor}}$  is the tensor kernel described previously. Note that the normalization factor  $\binom{k}{2}^{-1}$  from [23] is used, instead of DDC’s  $\frac{1}{k}$ .

Eqs. (2) and (3) constitute the mathematical formulation of the proposed unsupervised companion objectives. In essence, these are designed to enforce similar cluster structure at the outputs of each block in the network, ensuring a more consistent similarity structure between the outputs of subsequent blocks. Since the representational power of a single block is limited, and each block has its own companion objective, the similarity structure at later blocks should more closely resemble the similarity structure at the earlier blocks, compared to the unconstrained case.

### C. Model overview

An overview of the complete DTKC model is shown in Figure 3. The “FC” and “Out” layers as well as the losses  $\mathcal{L}_1$ ,  $\mathcal{L}_2$  and  $\mathcal{L}_3$  are from DDC, which has been shown to work well for both image clustering and time series clustering [4, 5], with randomly initialized parameters. Moreover, the companion objectives closely resemble DDC’s  $\mathcal{L}_1$ . The DDC loss function should therefore tend to agree with the companion objectives, so that they “pull in the same direction” during training. In order to strengthen this agreement, the normalization constant of  $\mathcal{L}_1$  was changed from  $\frac{1}{k}$  to  $\binom{k}{2}^{-1}$  in DTKC.

DTKC is trained end-to-end from randomly initialized parameters, using stochastic mini-batch gradient descent. The computational complexity of training is therefore linear in the number of images in the dataset.

Although DTKC shares its clustering module with DDC, it is important to emphasize that the unsupervised companion objectives can be coupled with any deep clustering algorithm, as long as it uses a deep neural network to produce the cluster membership predictions. The companion objectives have been introduced for tensors of arbitrary rank, meaning that they can be attached to any deep neural network which produces tensorial representations. To illustrate this generalizability, Appendix A includes some experiments where the companion objectives are used with a recurrent neural network to cluster sequential data.

## V. EXPERIMENTS

### A. Experiment setup

1) *Datasets*: We test the proposed DTKC model on the MNIST, USPS, SVHN, Fashion-MNIST, and COIL-100 datasets. These datasets represent clustering tasks which are often encountered in computer vision, and are thus widely used in the literature [6, 7, 14, 4, 2]. An overview of the datasets can be found in Table I.

Table I: Overview of the datasets used for evaluation.  $n$  and  $k$  denote the total number of images, and the number of categories, respectively.

Name	Image size	Color	$n$	$k$
MNIST [29]	$28 \times 28$	Gray	60000	10
USPS	$16 \times 16$	Gray	9298	10
SVHN [30]	$32 \times 32$	RGB	99289	10
Fashion-MNIST [31]	$28 \times 28$	Gray	60000	10
COIL-100 [32]	$128 \times 128$	RGB	7200	100

2) *Baseline models*: Several baseline algorithms were chosen to thoroughly assess the clustering performance of the proposed DTKC model. These algorithms include the well known  $k$ -means algorithm [33], and Spectral Clustering [15]. We also compare DTKC with the following Deep Clustering algorithms:

- Deep Divergence-based Clustering (DDC) [4].
- Deep Embedded Clustering (DEC) [6].
- SpectralNet [14].
- Improved Deep Embedded Clustering (IDEC) [7].
- Deep Clustering Network (DCN) [8].
- Discriminatively Boosted Clustering (DBC) [9].

The results for DDC and DEC were obtained by the authors of this paper<sup>3</sup>. The results for the remaining models were extracted from their respective publications, causing some missing entries in Table II.

3) *DTKC implementation*: Following [4, 6, 7, 8, 9], we use a relatively small network for our experiments. Our CNN consists of two sequential blocks, both having two convolutional layers with ReLU activation functions, followed by a  $2 \times 2$  max pooling operation. The convolutional layers each have 32 filters, with size  $5 \times 5$  in the first block, and  $3 \times 3$  in the second block. Batch normalization [34] was applied to the output of the last convolutional layer in each block. The first fully-connected layer has 100 units with ReLU activations. The output layer has number of units equal to the number of clusters, and uses a softmax activation function. See Fig. 3 for an overview of the model architecture.

DTKC was trained on stochastic mini-batches of size 120, using the Adam optimizer [35] with a learning rate of  $10^{-4}$ . Following [4], the model was trained from 20 different initializations, for a maximum of 100 epochs per run. A training run was terminated if no decrease in the loss function was observed over 30 epochs. The  $\sigma$  hyperparameter for each kernel was set to 15 % of the median pairwise distances between the activations from the respective layers, following [36, 4]. Finally, the  $\lambda$  hyperparameter was set to 0.01 for all experiments. See Section VI for further analysis on these parameter choices.

4) *Performance metrics*: We use the unsupervised clustering accuracy (ACC), and the normalized mutual information

<sup>3</sup>The DEC results were obtained using DEC-Keras <https://github.com/XifengGuo/DEC-keras> with the hyperparameters specified in [6].

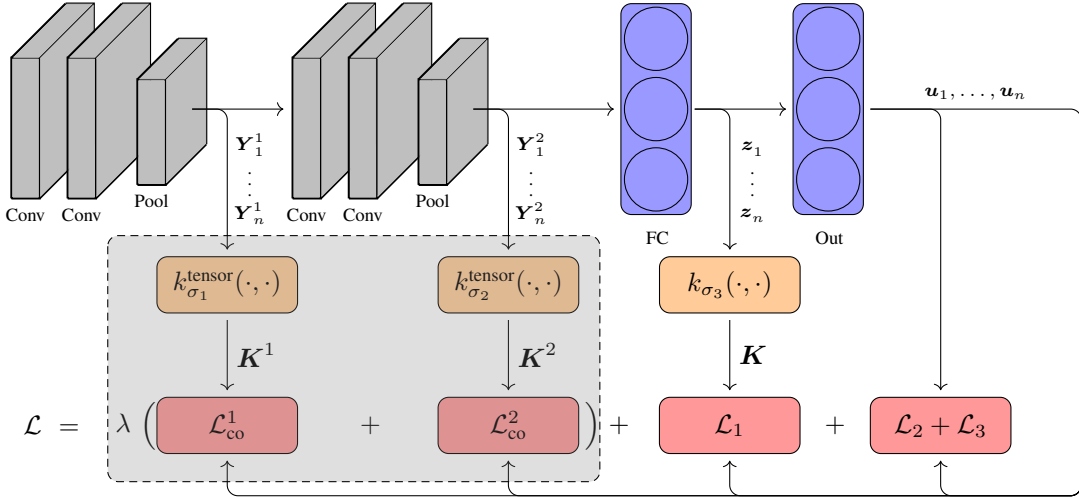


Figure 3: An overview of the DTKC model. The dashed box shows the computation of the proposed unsupervised companion objectives. The tensor kernels are computed from the outputs of each block, and then used to compute the companion objectives for the respective blocks.

(NMI) to measure the clustering performance of the different algorithms. The former is computed as:

$$ACC = \max_{m \in \mathcal{M}} \frac{1}{n} \sum_{i=1}^n \delta(m(y_i) - r_i)$$

where  $y_i = j : u_{ij} \geq u_{il}, l = 1, \dots, k$  is the predicted cluster for observation  $i$ , and  $r_i$  is the corresponding ground truth label for observation  $i$ .  $\delta(\cdot)$  denotes the Kronecker delta function, and  $\mathcal{M}$  denotes the set of all possible bijective mappings from  $\{1, \dots, k\}$  to itself. The maximum can be computed efficiently using the Hungarian algorithm [37]. The NMI is given by

$$NMI = \frac{I(\mathbf{y}, \mathbf{r})}{\frac{1}{2}(H(\mathbf{y}) + H(\mathbf{r}))}$$

where  $I(\cdot, \cdot)$  denotes the mutual information and  $H(\cdot)$  denotes the entropy.

The metrics were computed for the models resulting in the lowest value of the unsupervised loss function for each run. This resulted in 20 (ACC, NMI)-pairs, where each pair corresponds to the best observed performance for the given run, with respect to the loss function. These pairs were further aggregated to produce the following summary statistics:

- *Best*: ACC and NMI for the run which resulted in the lowest value of the loss function. This is used as the primary measure of model performance, as the best model is selected in a completely unsupervised manner.
- *Mean*: Average ACC and NMI over the 20 runs.
- *Sd.*: Standard deviation for ACC and NMI over the 20 runs.

## B. Results

Table II shows the performance of DTKC and the baseline models on the MNIST, USPS, and COIL-100 datasets. These results show that DTKC performs comparable to state of the art

Table II: Resulting ACC and NMI for the MNIST, USPS, and COIL-100 experiments. The best results are highlighted in bold.

	Model	ACC			NMI		
		Best	Mean	Sd.	Best	Mean	Sd.
MNIST	<i>k</i> -means	0.51	0.54	0.03	0.49	0.5	0.01
	Spectral Cl.	0.5	0.55	0.02	0.51	0.51	0.01
	DBC	0.96	–	–	<b>0.92</b>	–	–
	DCN	0.83	–	–	0.81	–	–
	IDEC	0.88	–	–	0.87	–	–
	SpectralNet	<b>0.97</b>	–	–	<b>0.92</b>	–	–
	DEC	0.83	<b>0.87</b>	0.03	0.85	<b>0.86</b>	0.01
	DDC	0.91	0.77	0.07	0.83	0.73	0.06
	DTKC	0.94	0.77	0.08	0.88	0.74	0.07
USPS	<i>k</i> -means	0.67	0.63	0.04	0.63	0.62	0.02
	Spectral Cl.	0.59	0.65	0.02	0.6	0.6	0.0
	DBC	0.74	–	–	0.72	–	–
	IDEC	0.76	–	–	0.78	–	–
	DEC	0.76	<b>0.76</b>	0.0	0.78	<b>0.78</b>	0.0
	DDC	<b>0.81</b>	0.69	0.06	0.77	0.7	0.03
	DTKC	0.78	0.7	0.06	<b>0.8</b>	0.73	0.05
COIL-100	<i>k</i> -means	0.62	<b>0.61</b>	0.01	0.83	0.83	0.0
	Spectral Cl.	0.44	0.56	0.05	0.76	0.81	0.02
	DBC	<b>0.78</b>	–	–	<b>0.91</b>	–	–
	DEC	0.59	<b>0.61</b>	0.02	0.84	<b>0.85</b>	0.01
	DDC	0.61	0.59	0.02	0.83	0.83	0.01
	DTKC	0.64	0.6	0.02	0.85	0.83	0.01

methods for deep clustering. The results also indicate that the deep clustering models significantly outperform the classical models for all datasets.

Note that, due to the generality of the unsupervised companion objectives, the goal of our approach is not necessarily to achieve the best overall clustering performance, but rather to see an improvement when adding the unsupervised companion objectives to a given base model. Thus, in order to more thoroughly investigate the effect of the unsupervised companion

Table III: Results for DDC and DTKC on all benchmark datasets.

	Model	ACC			NMI		
		Best	Mean	Sd.	Best	Mean	Sd.
MNIST	DDC	0.91	<b>0.77</b>	0.07	0.83	0.73	0.06
	DTKC	<b>0.94</b>	<b>0.77</b>	0.08	<b>0.88</b>	<b>0.74</b>	0.07
USPS	DDC	<b>0.81</b>	0.69	0.06	0.77	0.7	0.03
	DTKC	0.78	<b>0.7</b>	0.06	<b>0.8</b>	<b>0.73</b>	0.05
SVHN	DDC	0.15	0.14	0.01	0.02	0.02	0.01
	DTKC	<b>0.17</b>	<b>0.18</b>	0.01	<b>0.05</b>	<b>0.06</b>	0.01
F-MNIST	DDC	0.58	0.55	0.06	0.52	0.49	0.04
	DTKC	<b>0.63</b>	<b>0.56</b>	0.04	<b>0.55</b>	<b>0.5</b>	0.03
COIL-100	DDC	0.61	0.59	0.02	0.83	<b>0.83</b>	0.01
	DTKC	<b>0.64</b>	<b>0.6</b>	0.02	<b>0.85</b>	<b>0.83</b>	0.01

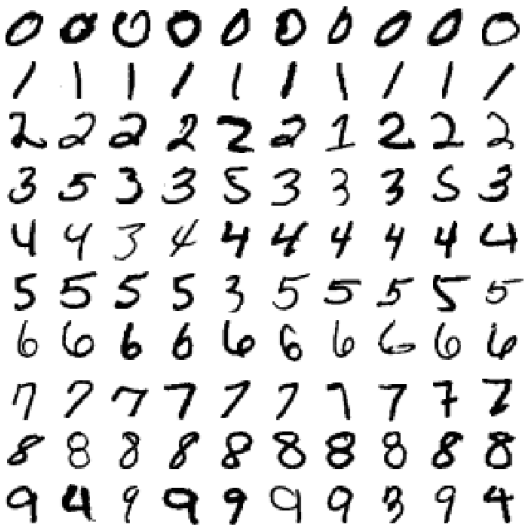


Figure 4: DTKC clustering results for randomly selected images from the MNIST dataset. Each row represents a cluster.

objectives, the resulting metrics for DDC and DTKC on all benchmark datasets, are listed in Table III. Here, DTKC outperforms DDC on all datasets, both in terms of mean performance, and in terms of best performance, for both metrics. The only exception is “best accuracy” on USPS, where DDC is somewhat better than DTKC. These results therefore indicate that the unsupervised companion objectives have helped guide DTKC towards clusterings that coincide better with the ground truth labels, compared to DDC.

Figure 4 shows examples from the clusters identified in the MNIST dataset. Each row in the figure corresponds to a distinct cluster, indicating that the model has indeed learned to group the images mostly based on the depicted digit. However, there are some notable errors, namely the mixing of threes and fives, and the mixing of fours and nines in the last cluster. The figure also shows a one assigned to the cluster of twos. Interestingly, this particular one has a horizontal bar at the bottom, as well as an oblique line at the top, making it more similar to the other twos.

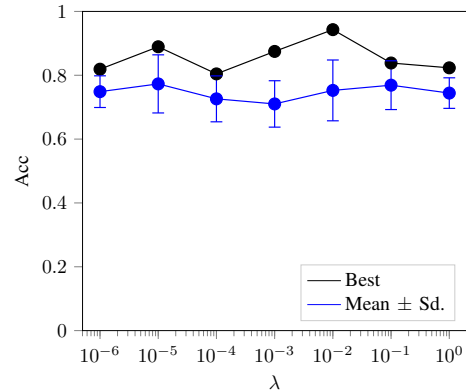


Figure 5: Effect of the  $\lambda$  hyperparameter on clustering accuracy for the MNIST dataset.

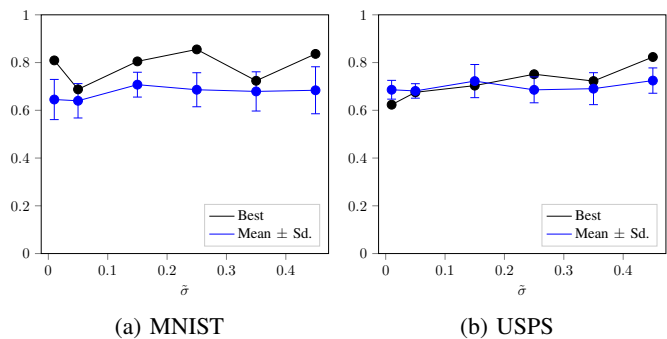


Figure 6: Effect of the  $\sigma$  hyperparameter on clustering accuracy for the MNIST and USPS datasets.

## VI. HYPERPARAMETER ANALYSIS

### A. Effect of the $\lambda$ hyperparameter

The specification of the strength of the unsupervised companion losses ( $\lambda$ ) is a both crucial and difficult task. In our experiments, we chose  $\lambda$  based on a supervised validation procedure on the MNIST benchmark dataset, and used the resulting value in all subsequent experiments. It is therefore important to examine how sensitive the model is to the choice of  $\lambda$ , since we expect our choice to generalize well to the other datasets included in the experiments.

The resulting accuracies for the DTKC model on the MNIST dataset are shown in Fig. 5. The plot does not show a particularly large variation in accuracy, but the optimal value seems to be at around  $\lambda = 0.01$ . The small variation implies that the model is rather robust to variations in  $\lambda$ . This property is especially important, as it makes the assumption about generalization to other datasets more feasible. Based on these observations, as well as the difficulties with unsupervised hyperparameter validation,  $\lambda$  was set to 0.01 for the remaining experiments.

### B. Effect of the $\sigma$ hyperparameter

Recall that the bandwidth parameter  $\sigma$  was chosen according to the “15 % of median distance” rule of thumb given in



[36]. This rule of thumb has been successfully applied to other DDC-based models [4, 5] – which is why it was used in our experiments as well. However, we know from the literature that the specification of  $\sigma$  in the Gaussian kernel can be difficult, as well as critical for the performance of the resulting algorithm [38]. The goal of this subsection is therefore to inspect the consequences of this choice, and more specifically, to investigate how sensitive the performance of DTKC is to variations in  $\sigma$ .

Note that the findings of this analysis were not used to specify the  $\sigma$  parameter, in contrast to what was done in the previous subsection for the  $\lambda$  hyperparameter. There are two main reasons for this, the first being that introducing a similar procedure for  $\sigma$  would result in a significant increase in the experimental complexity. The second reason is that for  $\sigma$ , we already have a rule of thumb which has been proven to work well with previous DDC-based models – which is not the case for the  $\lambda$  hyperparameter.

To evaluate the effect of different  $\sigma$  values on DTKC, the model was trained using variations of the aforementioned rule of thumb, on the MNIST and USPS datasets. Specifically, for a given layer  $l$ ,  $\sigma^l$  was varied according to:

$$\sigma^l = \tilde{\sigma} \cdot \text{median} \{d_{ij}^l\}_{i,j=1}^n$$

where  $\tilde{\sigma}$  is the multiplication factor<sup>4</sup>, and  $d_{ij}^l$  is the distance between output  $i$  and output  $j$  in layer  $l$ . Following the ordinary loss-function-computations, the tensor distance  $d_{\text{tensor}}(\cdot, \cdot)$  was used for the  $\sigma$  values in the companion objectives, while the Euclidean distance was used for  $\sigma$  in the DDC loss function. Note that the same  $\tilde{\sigma}$  was used for all layers, in order to reduce the complexity of the analysis.

The resulting accuracies are shown in Fig. 6. The accuracy plots show that the DTKC is rather robust towards variations in the multiplication factor  $\tilde{\sigma}$ . Thus indicating that the potential loss or gain in performance is not particularly large when varying this hyperparameter. This is indeed an advantage due to the difficulties often encountered with unsupervised hyperparameter selection.

## VII. VISUALIZATION OF IMPORTANCE

Importance visualization has become an important step when analyzing the results from deep learning models [39, 40, 41]. Figure 7 shows importance plots from DDC and DTKC for randomly selected digits from the MNIST dataset. The importance scores were obtained using SHAP [41].

The figure shows that the feature importances are very similar for the two models, and that both models focus on meaningful features in the input image. These features include e.g. the top horizontal bar in the fives and sevens, and the loop in the sixes. However, there are a few noteworthy differences between the two models. For instance, we observe that the three’s bottom curve has been assigned a higher importance in DTKC than in

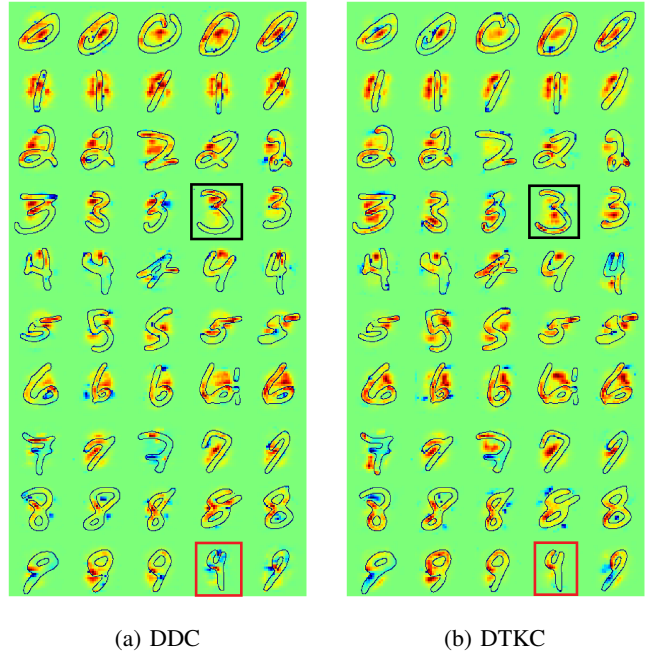


Figure 7: Importance

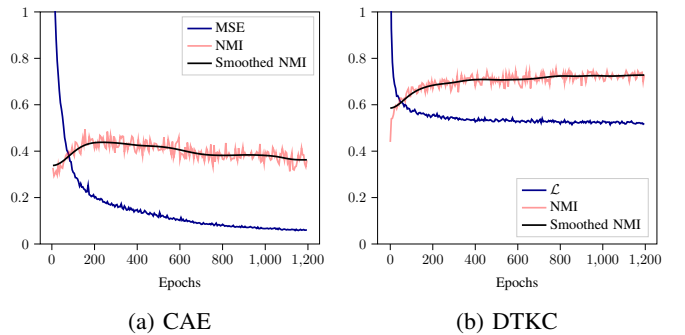


Figure 8: Loss and NMI for the experiments investigating objective function mismatch in a convolutional autoencoder [16], and in DTKC.

DDC (compare the digits framed in black). Another difference is the missing part of the loop in the red-framed nine, which has been assigned more negative importance in DDC, compared to DTKC.

## VIII. OBJECTIVE FUNCTION MISMATCH

To examine the potential objective function mismatch in autoencoder-based models, we train a convolutional autoencoder (CAE) [16] on the MNIST dataset for 1200 epochs, with a mean squared error (MSE) loss. The encoder part shares its architecture with DTKC, whereas the decoder is a mirrored version of the encoder, where the convolutions have been replaced with transpose convolutions, and the max-pooling operations have been replaced with nearest-neighbor up-sampling. During training, we extract the outputs of the second convolutional block every five epochs, and run  $k$ -means

<sup>4</sup>Note that setting  $\tilde{\sigma} = 0.15$  recovers the original rule of thumb.

on these representations. We then compute the NMI for each  $k$ -means clustering, resulting in 240 NMI values.

The resulting NMI values are shown in Fig. 8a as a function of epochs, along with the MSE loss. Here we can see that the NMI increases for the first 250 epochs, but starts to slowly decrease after this point, despite the continued decrease in MSE. This indicates that the later stages of the autoencoder training actually make the hidden representations more difficult to cluster, compared with the representations produced around epoch 250. This behavior shows the objective function mismatch between the autoencoder’s reconstruction objective, and the clustering objective.

Fig. 8b shows NMI values computed analogously during the training of DTKC. This plot shows a steady increase in NMI during training, and in contrast to the autoencoder case, no indication of objective function mismatch is visible.

## IX. CONCLUSION

We have proposed Deep Tensor Kernel Clustering (DTKC) – a new approach to image clustering with deep neural networks. At the heart of DTKC lie the unsupervised companion objectives, whose purpose are to guide the network towards a more consistent clustering structure at the outputs of its intermediate layers. Due to the tensorial nature of the intermediate representations in convolutional neural networks, we leverage the connection between tensor theory and CNNs, which allows us to use tensor kernels to quantify similarities between intermediate representations.

Our results indicate that the addition of these unsupervised companion objectives improves the clustering performance over several baseline models. Moreover, we demonstrate the presence of objective function mismatch when combining a convolutional autoencoder with a  $k$ -means clustering module – an effect which is not present in DTKC.

These results are indeed promising, but the preservation of geometrical structure in the input data is still a key challenge in deep clustering [7], and remains as an important direction for future work. To this end, the contributions made in this paper show that the quantification of cluster structure can be done for tensors of arbitrary rank. Promising work on e.g. increasing network efficiency [42], and tensor factorization [43, 44], indicate that there is still much untapped potential at the intersection between deep learning and tensor theory. More work along these lines can therefore lead to impactful advancements in the deep clustering field – especially for data types with more complex geometrical structure, such as images, sequences, and graphs.

## REFERENCES

- [1] Y. LeCun, Y. Bengio, and G. Hinton, “Deep Learning,” *Nature*, vol. 521, no. 7553, pp. 436–444, May 2015.
- [2] J. Yang, D. Parikh, and D. Batra, “Joint Unsupervised Learning of Deep Representations and Image Clusters,” in *International Conference on Computer Vision and Pattern Recognition*, 2016, pp. 5147–5156.
- [3] W. Hu, T. Miyato, S. Tokui, E. Matsumoto, and M. Sugiyama, “Learning Discrete Representations via Information Maximizing Self-Augmented Training,” in *International Conference on Machine Learning*, vol. 70, Aug. 2017, pp. 1558–1567.
- [4] M. Kampffmeyer, S. Løkse, F. M. Bianchi, L. Livi, A.-B. Salberg, and R. Jenssen, “Deep Divergence-Based Approach to Clustering,” *Neural Networks*, vol. 113, pp. 91–101, May 2019.
- [5] D. J. Trosten, A. S. Strauman, M. Kampffmeyer, and R. Jenssen, “Recurrent Deep Divergence-Based Clustering for Simultaneous Feature Learning and Clustering of Variable Length Time Series,” in *International Conference on Acoustics, Speech and Signal Processing*, May 2019, pp. 3257–3261.
- [6] J. Xie, R. Girshick, and A. Farhadi, “Unsupervised Deep Embedding for Clustering Analysis,” in *International Conference on Machine Learning*, ser. Proceedings of Machine Learning Research, vol. 48, Jun. 2016, pp. 478–487.
- [7] X. Guo, L. Gao, X. Liu, and J. Yin, “Improved Deep Embedded Clustering with Local Structure Preservation,” in *International Joint Conference on Artificial Intelligence*. Melbourne, Australia: International Joint Conferences on Artificial Intelligence Organization, Aug. 2017, pp. 1753–1759.
- [8] B. Yang, X. Fu, N. D. Sidiropoulos, and M. Hong, “Towards K-Means-Friendly Spaces: Simultaneous Deep Learning and Clustering,” in *International Conference on Machine Learning*, ser. Proceedings of Machine Learning Research, vol. 70, Aug. 2017, pp. 3861–3870.
- [9] F. Li, H. Qiao, and B. Zhang, “Discriminatively Boosted Image Clustering with Fully Convolutional Auto-Encoders,” *Pattern Recognition*, vol. 83, pp. 161–173, Nov. 2018.
- [10] L. Metz, N. Maheswaranathan, B. Cheung, and J. Sohl-Dickstein, “Meta-Learning Update Rules for Unsupervised Representation Learning,” Sep. 2018.
- [11] Y. Lecun, “Generalization and network design strategies,” in *Connectionism in perspective*. Elsevier, 1989.
- [12] M. Signoretto, “Kernels and Tensors for Structured Data Modelling,” PhD, Katholieke Universiteit Leuven – Faculty of Engineering, Dec. 2011.
- [13] C.-Y. Lee, S. Xie, P. W. Gallagher, Z. Zhang, and Z. Tu, “Deeply-Supervised Nets,” *Journal of Machine Learning Research*, vol. 38, 2015.
- [14] U. Shaham, K. Stanton, H. Li, R. Basri, B. Nadler, and Y. Kluger, “SpectralNet: Spectral Clustering Using Deep Neural Networks,” in *International Conference on Learning Representations*, 2018.
- [15] J. Shi and J. Malik, “Normalized Cuts and Image Segmentation,” *IEEE Transactions on Pattern Analysis and Machine Intelligence*, vol. 22, no. 8, pp. 888–905, Aug. 2000.
- [16] J. Masci, U. Meier, D. Cireşan, and J. Schmidhuber, “Stacked Convolutional Auto-Encoders for Hierarchical Feature Extraction,” in *Artificial Neural Networks and Machine Learning*. Berlin, Heidelberg: Springer Berlin Heidelberg, 2011, vol. 6791, pp. 52–59.
- [17] H. Noh, S. Hong, and B. Han, “Learning Deconvolution Network for Semantic Segmentation,” in *International Conference on Computer Vision*. Santiago, Chile: IEEE, Dec. 2015, pp. 1520–1528.
- [18] Z. Jiang, Y. Zheng, H. Tan, B. Tang, and H. Zhou, “Variational Deep Embedding: An Unsupervised and Generative Approach to Clustering,” in *International Joint Conference on Artificial Intelligence*, ser. IJCAI’17. AAAI Press, 2017, pp. 1965–1972.
- [19] D. P. Kingma and M. Welling, “Auto-Encoding Variational Bayes,” in *International Conference on Learning Representations*, Dec. 2014.
- [20] J. T. Springenberg, “Unsupervised and Semi-Supervised Learning with Categorical Generative Adversarial Networks,” *arXiv:1511.06390 [cs, stat]*, Nov. 2015.
- [21] I. Goodfellow, J. Pouget-Abadie, M. Mirza, B. Xu, D. Warde-Farley, S. Ozair, A. Courville, and Y. Bengio, “Generative Adversarial Nets,” in *Advances in Neural Information Processing Systems*. Curran Associates, Inc., 2014, vol. 27, pp. 2672–2680.

- [22] S. Mukherjee, H. Asnani, E. Lin, and S. Kannan, “ClusterGAN: Latent Space Clustering in Generative Adversarial Networks,” *Proceedings of the AAAI Conference on Artificial Intelligence*, vol. 33, pp. 4610–4617, Jul. 2019.
- [23] R. Jenssen, J. C. Principe, D. Erdogmus, and T. Eltoft, “The Cauchy–Schwarz Divergence and Parzen Windowing: Connections to Graph Theory and Mercer Kernels,” *Journal of the Franklin Institute*, vol. 343, no. 6, pp. 614–629, Sep. 2006.
- [24] E. Parzen, “On Estimation of a Probability Density Function and Mode,” *The Annals of Mathematical Statistics*, vol. 33, no. 3, pp. 1065–1076, Sep. 1962.
- [25] J. Hamm and D. D. Lee, “Grassmann Discriminant Analysis: A Unifying View on Subspace-Based Learning,” in *International Conference on Machine Learning*. ACM, 2008, pp. 376–383.
- [26] S. Jayasumana, R. Hartley, M. Salzmann, H. Li, and M. Harandi, “Kernel Methods on Riemannian Manifolds with Gaussian RBF Kernels,” *IEEE Transactions on Pattern Analysis and Machine Intelligence*, vol. 37, no. 12, pp. 2464–2477, Dec. 2015.
- [27] J. Zhang, G. Zhu, R. W. Heath Jr., and K. Huang, “Grassmannian Learning: Embedding Geometry Awareness in Shallow and Deep Learning,” *arXiv:1808.02229 [cs, eess, math, stat]*, Aug. 2018.
- [28] H. Anton and C. Rorres, *Elementary Linear Algebra: With Supplementary Applications*, 11th ed. Hoboken, NJ: Wiley, 2015.
- [29] Y. Lecun, L. Bottou, Y. Bengio, and P. Haffner, “Gradient-Based Learning Applied to Document Recognition,” *Proceedings of the IEEE*, vol. 86, no. 11, pp. 2278–2324, Nov. 1998.
- [30] Y. Netzer, T. Wang, A. Coates, A. Bissacco, B. Wu, and A. Y. Ng, “Reading Digits in Natural Images with Unsupervised Feature Learning,” in *Neural Information Processing Systems*, 2011, p. 9.
- [31] H. Xiao, K. Rasul, and R. Vollgraf, “Fashion-MNIST: A Novel Image Dataset for Benchmarking Machine Learning Algorithms,” Aug. 2017.
- [32] S. A. Nene, S. K. Nayar, and H. Murase, “Columbia Object Image Library (COIL-100),” Tech. Rep., Feb. 1996.
- [33] J. MacQueen, “Some Methods for Classification and Analysis of Multivariate Observations,” in *Berkeley Symposium on Mathematical Statistics and Probability, Volume 1: Statistics*. The Regents of the University of California, 1967.
- [34] S. Ioffe and C. Szegedy, “Batch Normalization: Accelerating Deep Network Training by Reducing Internal Covariate Shift,” in *International Conference on Machine Learning*, ser. ICML’15, vol. 37. JMLR.org, 2015, pp. 448–456.
- [35] D. P. Kingma and J. Ba, “Adam: A Method for Stochastic Optimization,” in *International Conference on Learning Representations*, 2015.
- [36] R. Jenssen, “Kernel Entropy Component Analysis,” *IEEE Transactions on Pattern Analysis and Machine Intelligence*, vol. 32, no. 5, pp. 847–860, May 2010.
- [37] H. W. Kuhn, “The Hungarian method for the assignment problem,” *Naval Research Logistics Quarterly*, vol. 2, no. 1-2, pp. 83–97, Mar. 1955.
- [38] G. H. Givens and J. A. Hoeting, *Computational Statistics*, 2nd ed., ser. Wiley Series in Computational Statistics. Hoboken, N.J: Wiley, 2013.
- [39] M. D. Zeiler and R. Fergus, “Visualizing and Understanding Convolutional Networks,” in *European Conference on Computer Vision*, ser. Lecture Notes in Computer Science. Springer International Publishing, 2014, pp. 818–833.
- [40] J. Springenberg, A. Dosovitskiy, T. Brox, and M. Riedmiller, “Striving for Simplicity: The All Convolutional Net,” in *International Conference on Learning Representations (workshop track)*, 2015.
- [41] S. M. Lundberg and S.-I. Lee, “A Unified Approach to Interpreting Model Predictions,” in *Advances in Neural Information Processing Systems 30*, I. Guyon, U. V. Luxburg, S. Bengio, H. Wallach, R. Fergus, S. Vishwanathan, and R. Garnett, Eds. Curran Associates, Inc., 2017, pp. 4765–4774.
- [42] V. Lebedev, Y. Ganin, M. Rakhuba, I. Oseledets, and V. Lempit- sky, “Speeding-up Convolutional Neural Networks Using Fine-Tuned CP-Decomposition,” *arXiv:1412.6553 [cs]*, Dec. 2014.
- [43] J.-T. Chien and Y.-T. Bao, “Tensor-Factorized Neural Networks,” *IEEE Transactions on Neural Networks and Learning Systems*, vol. PP, pp. 1–14, Apr. 2017.
- [44] S. Oymak and M. Soltanolkotabi, “End-to-End Learning of a Convolutional Neural Network via Deep Tensor Decomposition,” *arXiv:1805.06523 [cs, math, stat]*, May 2018.
- [45] K. Cho, B. van Merriënboer, C. Gulcehre, D. Bahdanau, F. Bougares, H. Schwenk, and Y. Bengio, “Learning Phrase Representations Using RNN Encoder–Decoder for Statistical Machine Translation,” in *Conference on Empirical Methods in Natural Language Processing*, Oct. 2014, pp. 1724–1734.
- [46] D. Dheeru and E. Karra Taniskidou, *UCI Machine Learning Repository*. University of California, Irvine, School of Information and Computer Sciences, 2017.
- [47] K. Ø. Mikalsen, F. M. Bianchi, C. Soguero-Ruiz, and R. Jenssen, “Time Series Cluster Kernel for Learning Similarities between Multivariate Time Series with Missing Data,” *Pattern Recognition*, vol. 76, pp. 569–581, Apr. 2018.
- [48] F. M. Bianchi, L. Livi, K. Ø. Mikalsen, M. Kampffmeyer, and R. Jenssen, “Learning Representations for Multivariate Time Series with Missing Data Using Temporal Kernelized Autoencoders,” *arXiv:1805.03473 [cs]*, May 2018.

## APPENDIX A

## EXPERIMENTS WITH SEQUENTIAL DATA

Up until this point, our focus has been on image clustering. However, in [5] it was shown that DDC provides a promising framework for the clustering of sequential data as well. By replacing the CNN with an RNN, it was shown that the resulting Recurrent Deep Divergence-based Clustering (RDDC) was able to outperform classical methods in sequence clustering. It is therefore natural to ask if the proposed framework can help improve the performance of RDDC as well, by introducing stronger supervision in earlier layers of the RNN.

Recall that RNNs can be regarded as layer-wise models, similarly to CNNs. The translation of the unsupervised companion objectives from CNNs to RNNs is therefore relatively straightforward. Suppose we have an input sequence  $\mathbf{x}_i = \mathbf{x}_{i,1}, \dots, \mathbf{x}_{i,T}$  where  $T$  is the length of the sequence. At layer  $l$  of the RNN we get the output sequence:

$$\mathbf{h}_{i,t}^l = f_{\theta_l}(\mathbf{h}_{i,t-1}^l, \mathbf{h}_{i,t}^{l-1}), \quad t = 1, \dots, T.$$

We can then use the last hidden states  $\mathbf{h}_{1,T}^l, \dots, \mathbf{h}_{n,T}^l$  of layer  $l$  to compute the companion objective. Note that in contrast to the CNN case, this will result in the companion objectives receiving rank-1 tensors (vectors) instead of rank-3 tensors. The regular Gaussian kernel was therefore used to compute the elements of the kernel matrix:

$$\mathbf{K}^l = [\kappa_{ij}^l], \quad \kappa_{ij}^l = \exp\left(-\frac{\|\mathbf{h}_{i,T}^l - \mathbf{h}_{j,T}^l\|^2}{2\sigma^2}\right)$$

*Models:* The sequential experiments were performed with two different models: RDDC as described in [5], and RDTKC (Recurrent Deep Tensor Kernel Clustering). The latter refers to a DTKC-based model where the CNN has been replaced with an RNN. Following [5] both models used a two-layer bidirectional gated recurrent unit [45], together with the DDC

Table IV: Summary of attributes for the sequential datasets. “Lengths” denotes the range of sequence lengths contained in the datasets.  $\text{dim}$ ,  $n$ , and  $k$  represent the dimensionality of each sequence-element, the number of sequences, and the number of clusters, respectively.

Name	Lengths	dim	$n$	$k$
Character Trajectories (CT)	[109, 198]	3	1491	10
Arabic Digits (AD)	[4, 93]	13	8800	10

Table V: Results for the experiments with sequential data.

	Model	ACC			NMI		
		Best	Mean	Sd.	Best	Mean	Sd.
CT	RDDC	0.64	0.58	0.09	0.73	0.68	0.09
	RDTKC	<b>0.8</b>	<b>0.65</b>	0.08	<b>0.83</b>	<b>0.74</b>	0.06
AD	RDDC	0.46	0.55	0.07	0.63	<b>0.62</b>	0.04
	RDTKC	<b>0.76</b>	<b>0.56</b>	0.09	<b>0.74</b>	0.61	0.07

clustering module. The dimensionality of the hidden states for each layer was set to 32, also following [5]. Batch size, optimizer, epochs, runs, and bandwidth all follow the configuration specified in Section V-A. The companion objectives in RDTKC were constructed as described above.

*Datasets:* To evaluate RDDC and RDTKC on sequential data, we use the first 10 characters from the Character Trajectories (CT) dataset [46], and all digits from the Arabic Digits dataset [46]. These datasets were chosen as they represent clustering or classification challenges of suitable complexity [5, 47, 48]. These are also openly accessible and well-known benchmark datasets, allowing for easier comparison with the literature. See Table IV for a summary of relevant attributes.

*Results:* The results for the sequential experiments are given in Table V. These results show that the addition of the unsupervised companion objectives in RDTKC has led to increased clustering performance, compared to RDDC.